Unphosphorylated *Rhabdoviridae* Phosphoproteins Form Elongated Dimers in Solution†

Francine C. A. Gerard,‡ Euripedes de Almeida Ribeiro Jr.,‡ Aurélie A. V. Albertini,‡,§ Irina Gutsche,‡ Guiseppe Zaccai,|| Rob W. H. Ruigrok,‡ and Marc Jamin*,‡

Unit of Virus Host Cell Interactions, UMR 5233 UJF-EMBL-CNRS, 6 rue Jules Horowitz, 38042 Grenoble Cedex 9, France, and Institut Laue Langevin, 6 Rue Jules Horowitz BP 156, 38042 Grenoble Cedex 9, France

Received April 25, 2007; Revised Manuscript Received June 27, 2007

ABSTRACT: The phosphoprotein (P) is an essential component of the replication machinery of rabies virus (RV) and vesicular stomatitis virus (VSV), and the oligomerization of P, potentially controlled by phosphorylation, is required for its function. Up to now the stoichiometry of phosphoprotein oligomers has been controversial. Size exclusion chromatography combined with detection by multiangle laser light scattering shows that the recombinant unphosphorylated phosphoproteins from VSV and from RV exist as dimers in solution. Hydrodynamic analysis indicates that the dimers are highly asymmetric, with a Stokes radius of 4.8−5.3 nm and a frictional ratio larger than 1.7. Small-angle neutron scattering experiments confirm the dimeric state and the asymmetry of the structure and yield a radius of gyration of about 5.3 nm and a cross-sectional radius of gyration of about 1.6−1.8 nm. Similar hydrodynamic properties and molecular dimensions were obtained with a variant of VSV phosphoprotein in which Ser60 and Thr62 are substituted by Asp residues and which has been reported previously to mimic phosphorylation by inducing oligomerization and activating transcription. Here, we show that this mutant also forms a dimer with hydrodynamic properties and molecular dimensions similar to those of the wild type protein. However, incubation at 30 °C for several hours induced self-assembly of both wild type and mutant proteins, leading to the formation of irregular filamentous structures.

Viruses of the *Rhabdoviridae* family form enveloped particles that possess a nonsegmented single-stranded negative sense RNA genome. Together with the *Paramyxoviridae* (measles, parainfluenza, respiratory syncytial, Hendra, and Nipah viruses), *Bornaviridae*, and *Filoviridae* (Ebola and Marburg viruses) families, they constitute the order of *Mononegavirales* (*MNV*) that includes many human, animal, and plant pathogens (*1*). *MNV* viruses exhibit a great diversity in terms of morphology and interactions with their hosts, but they share similar genomic and structural organizations as well as similar modes of RNA replication and transcription (*1*). The linear viral RNA genome is tightly associated with the viral nucleoprotein (N)[1] in a helical ribonucleoprotein complex (RNP) (*2*, *3*) that serves as template for both transcription and replication (*4*). The genomes comprises five common genes, which are similarly organized along the RNA molecule for all *MNV* viruses, encoding successively the N, the phosphoprotein (P), the matrix protein (M), the glycoprotein (G), and the RNA-dependent RNA polymerase (L). For rabies virus (RV) and vesicular stomatitis virus (VSV), only three of these proteins, N, P, and L, are necessary for synthesizing viral RNA in an efficient and regulated manner (*5*, *6*). Among those three, P has multiple functions during the replication cycle and is required for RNA synthesis and encapsidation of the viral RNA by N. P binds to nascent nucleoproteins, acting as a chaperone by forming RNA-free N°−P complexes necessary for encapsidation of new viral genomes (*7*, *8*). P also acts as a cofactor of the viral RNA polymerase, forming a two-subunit RNA polymerase complex in which L carries out all the enzymatic activities of RNA-dependent RNA transcription and replication, including mRNA cap synthesis and mRNA polyadenylation (*5*, *9*, *10*). By binding to both L and N, P allows the RNA polymerase complex to bind to RNPs. However, little is known about the mechanisms of action of this protein, and P could also be involved in the remodeling of RNPs during RNA synthesis (*2*).

Oligomerization of P is a common property among viruses of the *MNV* order. For some members of the *Paramyxoviridae* family (subfamily of the *Paramyxovirinae*: Sendai virus,

† This work was supported by the interdisciplinary program "Maladies Infectieuses Emergentes" from the CNRS. F.C.A.G. and A.A.V.A were supported by MENRT fellowships from the French government. E.d.A.R. was supported by a postdoctoral fellowship from the Université Joseph Fourier, Grenoble.

* Corresponding author: Unit of Virus Host Cell Interactions (UVHCI), UMR 5233 UJF-EMBL-CNRS, 6, rue Jules Horowitz, B.P. 181, 38042 Grenoble Cedex 9, France. E-mail: jamin@embl.fr. Phone: + 33 4 76 20 94 62. Fax: + 33 4 76 20 94 00.

‡ Unit of Virus Host Cell Interactions, UMR 5233 UJF-EMBL-CNRS.

§ Present address: CNRS, UMR2472, INRA, UMR1157, IFR115, Laboratoire de Virologie Moléculaire et Structurale, 91198, Gif sur Yvette, France.

|| Institut Laue Langevin.

[1] Abbreviations: AUC, analytical ultracentrifugation; CHPV, Chandipura virus; DLS, dynamic light scattering; HPLC, high-pressure liquid chromatography; MALLS, multiangle laser light scattering; N, nucleoprotein; P, phosphoprotein; RV, rabies virus; SANS, small-angle neutron scattering; SDS−PAGE, sodium dodecyl sulfate polyacrylamide gel electrophoresis; SEC, size-exclusion chromatography; VSV, vesicular stomatitis virus.

10.1021/bi7007799 CCC: $37.00 © 2007 American Chemical Society
Published on Web 08/17/2007

measles virus), the oligomerization domain is required for transcription and replication, and oligomerization is not controlled by phosphorylation (*11*, *12*). For other members of this family, phosphorylation of P is required for its oligomerization and transcriptional activity (*13*, *14*). In the *Rhabdoviridae* family, studies with RV and VSV have provided unclear pictures about the state of oligomerization and of phosphorylation required for the activities of the phosphoprotein. Studies with VSV (*Vesiculovirus* genus) indicate that oligomerization of P is required for binding to L polymerase and to N-RNA template (*15*−*17*) and for transcriptional activity (*18*−*20*). Oligomerization is controlled by phosphorylation in the N-terminal region of the protein (*18*−*20*) and by protein concentration (*21*). Conversely, phosphorylation in the N-terminal region is not required for the formation of RNA-free N°−P complexes and for RNA replication (*8*, *21*, *22*). The three-dimensional structure of the central domain of VSV P is dimeric (*23*), but biochemical studies have suggested that unphosphorylated P is monomeric and that phosphorylated P forms dimers, trimers, or tetramers (*19*, *24*, *25*). Recent data support the existence of different RNA polymerase complexes involved in transcription and replication (*26*, *27*), and it is possible that phosphorylation of P acts as a switch between these activities. Substitution of the phosphorylation sites indicates that phosphorylation is not strictly required for transcription and replication of the RNA, but that it stimulates these activities by favoring oligomerization (*19*, *21*). Also, the replacement of two phosphorylation sites by Asp in the N-terminal region was shown to mimic phosphorylation in its ability to induce oligomerization and transcriptional activity (*19*). Studies with Chandipura virus (CHPV), another *Vesiculovirus*, show that unphosphorylated P is inactive in transcription and exists in a concentration-dependent monomer−dimer−tetramer equilibrium (*28*). Phosphorylation of a single residue in the N-terminal region induced a large conformational change in the protein (*29*, *30*), stabilized the dimeric form (*16*), and activated transcription (*31*). In studies with RV, belonging to another genus (*Lyssavirus* genus) of the *Rhabdoviridae* family, different oligomeric forms of unphosphorylated P were found in solution, suggesting that phosphorylation of P is not required for oligomerization (*32*). The absence of an *in vitro* transcription system for rabies virus precluded, however, the characterization of the role of P in RNA transcription and replication. Throughout this ensemble of studies, the stoichiometry of the different phosphorylated and unphosphorylated forms of P from both viruses remained unclear, and controversial results have been obtained by different approaches (*19*, *25*, *32*).

In order to characterize the stoichiometry and molecular dimensions of the unphosphorylated form of VSV and RV P, we used size-exclusion chromatography, multiangle static light scattering, dynamic light scattering, analytical ultracentrifugation, and small-angle neutron scattering. To investigate the effect of phosphorylation on the oligomerization of VSV P, we characterized the properties of a variant of this protein in which two phosphorylation sites (S60 and T62) were substituted by aspartate residues, substitutions that have been shown previously to mimic a constitutive phosphorylated state of the protein. Our results indicated that, at 20 °C, both WT and mutant proteins form highly asymmetric dimers and convert to large oligomers (>700 kDa) in a temperature-dependent cooperative process.

MATERIALS AND METHODS

Production and Purification of Recombinant P Proteins. The phosphoprotein from the Orsay strain (Indiana serotype) of VSV (VSV P) was expressed using a recombinant plasmid pET22b+ containing the full length gene with a His-Tag at its C-terminal end (a gift from Dr. Blondel, Gif-sur-Yvette). A second plasmid for expressing the S60D/T62D double mutant of VSV P was constructed by introducing mutations at positions 60 and 62 by PCR site-directed mutagenesis using an inverse PCR method (Quickchange, Stratagene). The sequences of both P genes were verified by standard dideoxy sequencing. Each plasmid was transformed into *Escherichia coli* BL21 (DE3) pLysS strain, and the cells were grown in Luria−Bertoni medium at 37 °C until OD 600 nm reached 0.3. Expression of the recombinant protein was then induced with 0.5 mM isopropyl-1-thio-β-D-galactopyranoside (IPTG) for 5 h at 25 °C. Cells were harvested by centrifugation and then suspended in lysis buffer containing 20 mM Tris-HCl, 150 mM NaCl at pH 7.5. The cells were disrupted by sonication on ice. The cell debris was removed by centrifugation for 1 h at 20000*g*, 4 °C. The supernatant was filtered over a 0.2 μm membrane and loaded onto a Ni^{2+} charged affinity column (Sigma). The column was washed with 20 mM Tris-HCl, 500 mM NaCl buffer at pH 7.5, and P was eluted with 400 mM imidazole. Fractions containing P were pooled and concentrated on a unit concentration cell (Amicon, cutoff 10 kDa, Millipore) and then applied onto a Hiload 16/60 Superdex 200 column equilibrated with 20 mM Tris-HCl, 150 mM NaCl buffer at pH 7.5 (GE Healthcare). The purity of the protein preparation was checked by 12% Tris-Tricine SDS−PAGE. Identification by immunodetection was done with a rabbit polyclonal antibody (a gift from Dr. J. Curran, Geneva) and a secondary anti-rabbit antibody coupled to alkaline phosphatase. Circular dichroism spectra for both proteins were identical and similar to those published previously (data not shown) (*25*). The identity and integrity of both VSV proteins were confirmed by electrospray mass spectrometry. The experiments were performed on a Quattro II mass spectrometer (Micromass, Altricham, U.K.) by continuously injecting the sample with a Type 22 pump from Harvard Apparatus at a flow rate of 5 μL.min^{-1}. VSV P and ST VSV P were at a concentration of 1 mg mL^{-1} in H_2O containing 1% formic acid. The measured molecular masses are 30 975 ± 7 Da and 31 016 ± 5 Da for expected molecular mass calculated from the amino acid sequence including the His-tag of 30 976 Da and 31 018 , respectively.

The phosphoprotein from the CVS strain of rabies virus (RV P) was produced in insect cells (High Five) and purified according to the protocol described previously (*33*, *34*). The purity of the protein preparation was checked by 12% Tris-Tricine SDS−PAGE, and identification by immunodetection was done with a mouse monoclonal antibody (25E6) (a gift from Dr. D. Blondel, Gif-sur-Yvette) and a secondary anti-mouse antibody coupled with alkaline phosphatase. Electrospray mass spectrometry revealed a major species with a molecular mass of 33 520 ± 7 Da for and a minor species with a molecular mass of 33 596 Da that could correspond to a phosphorylated form of the protein (expected molecular mass calculated from the amino acid sequence: 33 616 Da).

Analytical Size Exclusion Chromatography and Multiangle Laser Light Scattering. Size exclusion chromatography (SEC) was performed with a S200 Superdex column (GE Healthcare). The column was equilibrated in 20 mM Tris-HCl, 150 mM NaCl buffer at pH 7.5. Separations were performed at 20 °C with a flow rate of 0.5 mL min^{-1}. Typically, 20 μL of protein solution at a concentration of 3−5 mg mL^{-1} was injected. The excluded (V_0) and total volumes (V_t) were measured with blue dextran and thymidine, respectively. The partition coefficients (K_{av}) were calculated by using

$$K_{av} = \frac{V_e - V_0}{V_t - V_0} \quad (1)$$

where V_e is the elution volume of the protein. The column was calibrated using proteins of known Stokes radii (R_S) and molecular mass (M_w) (*35*): myoglobin (R_S = 2.10 nm, M_w = 17 kDa), chymotrypsinogen (R_S = 2.28 nm, M_w = 25 kDa), bovine serum albumine (R_S = 3.37 nm, M_w = 67 kDa), aldolase (R_S = 4.65 nm, M_w = 158 kDa), catalase (R_S = 5.21 nm, M_w = 232 kDa), ferritine (R_S = 6.80 nm, M_w = 440 kDa), and thyroglobulin (R_S = 7.85 nm, M_w = 669 kDa) (*35*).

On-line MALLS detection was performed with a DAWN-EOS detector (Wyatt Technology Corp., Santa Barbara, CA) using a laser emitting at 690 nm. For each point on the HPLC chromatogram, the amount of light scattered is directly proportional to the product of protein concentration and molar mass, according to Zimm's formula for a diluted polymer solution (*36*, *37*):

$$\frac{R_\theta}{K^*C} = MP(\theta) - 2A_2CM^2P^2(\theta) \quad (2)$$

where R_θ is the measured excess Rayleigh's ratio, C is the protein concentration (g mL^{-1}), M is the molar mass (g mol^{-1}), $P(\theta)$ is the form factor, which depends on the structure of the scattering particles and describes the angular dependence of the scattered light, and A_2 is the second virial coefficient. K^* is an optical constant given by the following equation:

$$K^* = \frac{1}{N_A}\left(\frac{2\pi n_0}{\lambda^2}\right)^2\left(\frac{dn}{dc}\right)^2 \quad (3)$$

where N_A is Avogadro's number, n_0 is the refractive index of the solvent at the incident radiation wavelength (1.33 for a diluted aqueous buffer), dn/dc (mL g^{-1}) is the specific refractive index increment of the solute, and λ is the wavelength of the incident light in void. For particles smaller than the incident wavelength, no angular dependence is observed ($P(\theta) = 1$), and for a sufficiently diluted solution, A_2 is negligible ($A_2 = 0$). Equation 2 then simplifies and Rayleigh's ratio only depends on protein concentration and molar mass:

$$\frac{R_\theta}{K^*C} = M \quad (4)$$

The molar mass, M, can thus be calculated if C is known. Protein concentration was measured on-line by refractive index measurements using an RI2000 detector (Schambeck SFD) and refractive index increment dn/dc = 0.185 mL g^{-1}. Within the elution peak, the chromatogram is divided in slices, and for each slice, MALLS and refractive index measurements are used to calculate the molar masses using eq 4. The number-averaged (M_n) and weight-averaged (M_w) molar mass are obtained from the molar mass distribution across the elution peak. Analysis of the data was performed with the ASTRA software (Wyatt Technology Corp., Santa Barbara, CA).

Dynamic Light Scattering. Samples with protein concentrations ranging from 0.5 to 3.0 mg mL^{-1} were centrifuged for 10 min at 13000*g* and filtered through a 0.1 μm cutoff membrane filter in order to eliminate dust and large aggregates. Dynamic light scattering was measured at a scattering angle of 90° on a Dynapro apparatus (ProteinSolutions) using a 20 μL cuvette and a laser emitting at λ = 835.6 nm. Data were analyzed with the Dynamics v5.26.41 software. The "baseline limit" parameter was used to reject initial measurements. The apparent translational diffusion coefficients, D, obtained from the autocorrelation function, were converted into hydrodynamic radii (R_S) according to the Stokes−Einstein equation:

$$R_S = \frac{RT}{N_A 6\pi\eta_0 D} \quad (5)$$

where R is the gas constant, T is the temperature, N_A is Avogadro's number, and η_0 is the solvent viscosity. Control experiments carried out with lysozyme yielded the expected apparent translational diffusion coefficient.

Sedimentation Velocity Measurements. Sedimentation velocity experiments were performed in a Beckman XL1 ultracentrifuge at rotor speed of 42 000 rpm and at 20 °C using Epon charcoal-filled 12 or 3 mm double-sector centerpieces. Radial absorbance scans (λ = 280 nm) were acquired every 3 or 10 min. The program SEDFIT (*38*) (available from the RASMB Web site, http://www. bbri.org/rasmb/rasmb.html) was used to model the sedimentation profiles using the integrated Lamm equation solutions:

$$A(r,t) = \int c_0(s)\,\chi(s,D,r,t)\,ds + \epsilon + \delta \quad (6)$$

where $A(r,t)$ is the absorbance at radius r and time t, s and D are sedimentation and diffusion coefficients, c_0 is the loading concentration of protein, χ is the sedimentation profile (i.e., boundary), and ϵ and δ are signal offsets (the first term accounts for systematic errors, and the second term accounts for random errors). Sedimentation coefficient values between 0.5 and 15 S were resolved using maximum entropy regularization with a 0.68 confidence level. The relationships between the molecular mass, M_w, the sedimentation coefficient, s, the diffusion coefficient, D, and the Stokes radius, R_S, are obtained using the Svedberg equation (*37*, *39*),

$$D = \frac{sRT}{M_w(1 - \bar{\nu}\rho_0)} \quad (7)$$

and by combining this equation with eq 5:

$$R_S = \frac{M_w(1 - \bar{\nu}\rho_0)}{6\pi\eta_0 s} \quad (8)$$

Knowledge of s and M_w or of s and D allows the evaluation of the translational friction ratio f/f_0, where f_0 is the

translational friction coefficient for a sphere of the same mass and anhydrous volume, according to the following equations (*37*):

$$\frac{f}{f_0} = \frac{M_w(1 - \bar{\nu}\rho_0)}{N_A 6\pi\eta_0 s\left(\frac{3M_w\bar{\nu}}{4\pi N_A}\right)^{1/3}} \quad (9a)$$

$$\frac{f}{f_0} = \frac{RT}{N_A 6\pi\eta_0 D\left(\frac{3M_w\bar{\nu}}{4\pi N_A}\right)^{1/3}} \quad (9b)$$

Solvent density (ρ_0) of 1.005 g mL^{-1}, solvent viscosity (η_0) of 1.0214 cP, and the partial specific volume ($\bar{\nu}$) of VSV P and RV P of 0.726 and 0.732 mL g^{-1} were calculated at 20 °C with Sednterp (http://www.bbri.org/RASMB/rasmb.html). Intrinsic sedimentation and diffusion coefficients ($s^0_{20,w}$ and $D^0_{20,w}$) corrected to water at 20 °C were calculated from the experimental s_{mes} and D_{mes} values obtained in the experimental solvent and temperature conditions according to

$$s^0_{20,w} = s_{mes}\left(\frac{\eta_{20,w}}{\eta_{T,b}}\right)\left(\frac{1 - \bar{\nu}\rho_{T,b}}{1 - \bar{\nu}\rho_{20,w}}\right) \quad (10a)$$

$$D^0_{20,w} = D_{mes}\left(\frac{\eta_{20,w}}{\eta_{T,b}}\right) \quad (10b)$$

where $\eta_{20,w}$ and $\eta_{T,b}$ are the water viscosity at 20 °C and buffer viscosity at the experimental temperature and $\rho_{20,w}$ and $\rho_{T,b}$ are the water density at 20 °C and the buffer density at the experimental temperature.

Small-Angle Neutron Scattering (SANS). SANS experiments were performed on the D22 beam-line at the Institut Laue-Langevin (ILL, Grenoble, France). Neutron wavelength of 0.6 nm and a sample-to-detector distance of 4 m were used to cover the range 0.11 nm^{-1} ≤ Q ≤ 2.4 nm^{-1}. Protein concentration was 5 mg/mL. Scattering data were radially averaged about the beam center, corrected for transmission, corrected by subtracting empty cell and solvent scattering, and calibrated on an absolute scale by using the scattering of 0.100 cm of water (*40*).

Analysis of the scattering curves at small Q values using the Guinier approximation gives the radius of gyration (R_g) and the forward scattering intensity at zero Q (I_0) according to (*37*, *41*)

$$I(Q) = I_0 \exp\left(\frac{-R_g{}^2Q^2}{3}\right) \quad (11)$$

The scattering amplitude, Q, is given by the following equation:

$$Q = \frac{4\pi\sin\theta}{\lambda} \quad (12)$$

where 2θ is the scattering angle and λ is the wavelength. The radius of gyration was calculated from the initial slope of the plot of ln(I) versus Q^2. The molecular mass of the particles, M_w, was directly calculated from the forward intensity, I_0, knowing the protein concentration and the scattering length density (*40*).

$$M_w = \frac{I(0)N_A}{c(\Delta\rho\bar{\nu})^2} \quad (13)$$

where N_A is Avogadro's number, c is the protein concentration in mg mL^{-1}, $\Delta\rho$ is the difference, $\rho - \rho_0$, between the scattering length density of the molecule, ρ, and the scattering length density of the solvent, ρ_0, and $\bar{\nu}$ is the partial specific volume of the protein.

If one of the molecular dimensions is longer than the other two, the radius of gyration of the cross-section, R_c, can be obtained from the plot of the ln(I·Q) versus Q^2 (*41*), according to the following equation:

$$\ln[I(Q\cdot Q)] = \ln[I(Q\cdot Q)]_{Q\to 0} - \frac{R_c{}^2Q^2}{2} \quad (14)$$

and triaxial molecular dimensions were calculated by using R_g and R_c values derived from Guinier and cross-sectional analysis (*41*). Assuming a cylindrical shape for P proteins, the length of the cylinder, L, is given by

$$L = \sqrt{12(R_g{}^2 - R_c{}^2)} \quad (15)$$

and the radius, r, is given by

$$r = \sqrt{2}R_c \quad (16)$$

The data for Q values ranging from 0.11 to 1.0 nm^{-1} were used with the GNOM program (*42*) to determine the distance distribution function, $P(r)$, the radius of gyration, R_g, and the forward intensity, $I(0)$. The maximum dimension, D_{max}, required in this procedure and beyond which $P(r) = 0$, was selected such that the $P(r)$ function remained stable.

Oligomerization of P and Electron Microscopy. Samples of VSV P and ST VSV P proteins at 2.6 mg mL^{-1} were incubated in 20 mM Tris/HCl, 150 mM NaCl, pH 7.5 at 30 °C for different times. The kinetics of disappearance of the dimers and of appearance of the large oligomers of P at 30 °C were fitted to second-order rate equation using SigmaPlot (SPSS Inc., Chicago, IL). Samples obtained after incubation in those conditions for 1 or 3.5 h were used for electron microscopy. These samples were diluted to a concentration of about 0.1 mg mL^{-1}, adsorbed onto the clean face of a carbon film deposited on a mica sheet, negatively stained with 1% (w/v) uranyl acetate, and observed under low-dose conditions with a JEOL 1200 EX II microscope at 100 kV and a nominal magnification of 40000×.

RESULTS

Stoichiometry of P Protein Oligomers in Solution. Recombinant VSV P and its S60D/T62D variant (ST VSV P) were expressed in *E. coli*, and RV P was expressed in insect cells. All three proteins were purified as full-length proteins as shown by mass spectrometry. They elute from a Superdex 200 (GE Healthcare) SEC column as single peaks (Figure 1). The absolute molecular mass was determined at each point of the chromatograms by combining detections by MALLS and refractometry (eq 4). For all of these P proteins, the molecular mass is constant across the elution peak (Figure 1), and the polydispersity factor (M_w/M_n) is equal to 1.00 ± 0.05, indicating monodisperse species. The weight-average

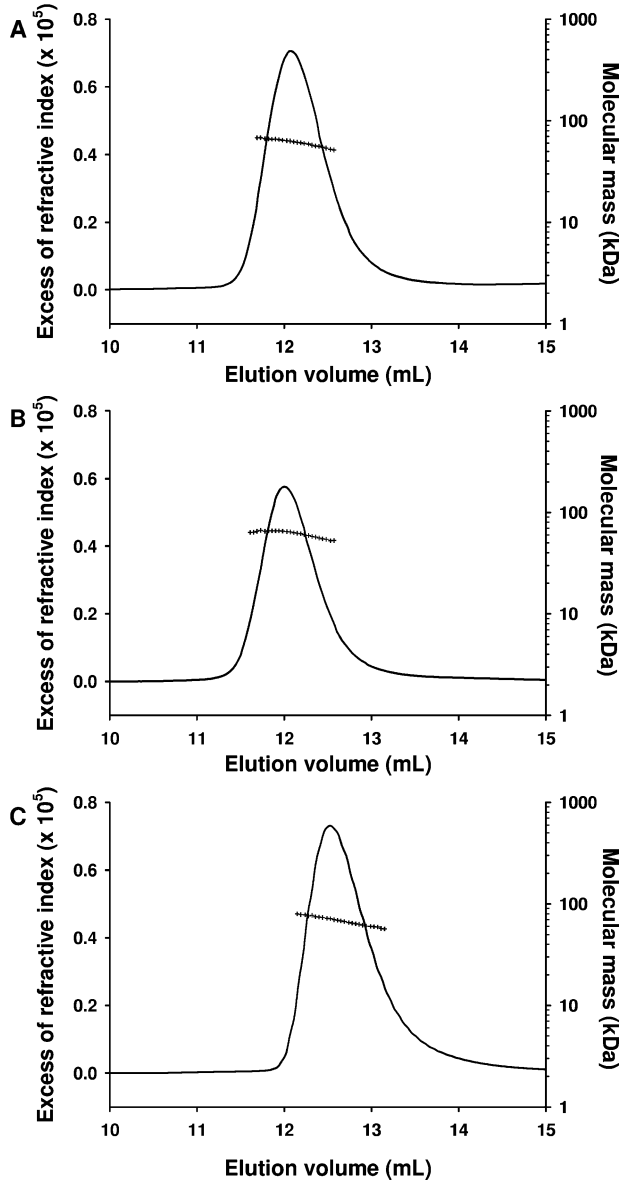

FIGURE 1: Molecular mass of phosphoprotein determined by multiangle laser light scattering and refractometry combined with size-exclusion chromatography. (A) VSV P, (B) ST VSV P, and (C) RV P. SEC was performed on a Superdex 200 column (300 mm × 10 mm) (GE Healthcare), equilibrated in 20 mM Tris-HCl, 150 mM NaCl buffer at pH 7.5. Separations were performed at 20 °C with a flow rate of 0.5 mL min^{-1}. 50 μL of a protein solution at 3−5 mg mL^{-1} was injected. The line shows the elution profile monitored by excess refractive index (left ordinate axis). The crosses (+) show the molecular mass distribution (right ordinate axis) determined from MALLS and refractometry data. Detectors at 60°, 69°, 80°, 90°, 100°, 111°, and 121° were used for the analysis, and the light scattering profile displays no angular dependence.

(M_w) molecular mass values are 61 ± 2 kDa, 63 ± 3 kDa, and 69 ± 2 kDa for VSV P, ST VSV P, and RV P, respectively, demonstrating that the three P proteins form dimers in solution (molecular masses of dimeric P proteins calculated from the sequence are 61 952 Da, 62 018 Da, and 67 232 Da, respectively) (Table 1 and Figure 1). No significant variation of the average molecular mass is observed for concentrations ranging from 100 to 645 μM, and the elution volume is identical for protein concentrations ranging from 20 μM to 645 μM (data not shown). Similar results (see below) confirming that P proteins form dimers were obtained from small-angle neutron scattering experiments (SANS) and also by combining results from sedimentation velocity, SEC, and DLS (Table 1).

Some of our samples of RV P contained a small population (near 5%) of other species eluting from the SEC column at smaller volumes than RV P dimers. These species migrate differently than the major species on SDS−PAGE in the absence of a reducing agent. RV P contains two cysteine residues, and most of these additional species disappear upon addition of a reducing agent, suggesting that they result from the formation of intermolecular disulfide bonds (data not shown).

Hydrodynamic Properties. The Stokes radii of the three P proteins were determined by SEC using globular proteins of known R_S for calibration (Figure 2). Values of 5.2 ± 0.1 nm, 5.3 ± 0.1 nm, and 4.8 ± 0.1 nm were obtained for VSV P, ST VSV P, and RV P, respectively (Table 2). These values are larger than those expected for a globular protein of the size of P monomers or even of P dimers. The R_S(measured)/R_S(globular) ratio, where R_S(globular) is the Stokes radius for a globular protein of about 65 kDa (dimer), is of the order of 1.65−1.70, indicating that P dimers are nonspherical and/or partially disordered. Similar results were obtained with a Superose 12 column (data not shown).

Dynamic light scattering, measured at a protein concentration of 80 μM, shows that both VSV P and ST VSV P are monodisperse species with translational diffusion coefficient ($D_{20,w}$) values of 4.27 ± 0.08 10^{-7} cm s^{-2} and 4.15 ± 0.08 10^{-7} cm s^{-2}, respectively (Table 2). Hydrodynamic radii, R_S, calculated according to the Stokes−Einstein equation (eq 5), are in good agreement with the values measured by SEC (Table 2). With RV P, the DLS measurements indicate the presence of several species, with a major component exhibiting a D value of 4.48 ± 0.10 10^{-7} cm s^{-2}, also in good agreement with the value measured by SEC.

The hydrodynamic properties of the three P proteins were finally characterized by sedimentation velocity experiments at three different protein concentrations. Small amounts of large aggregates corresponding to 5 to 15% of the absorbance signal are detected at low protein concentrations (0.25 mg mL^{-1} and 1 mg mL^{-1}) as species that sediment very rapidly (s of about 60 S), whereas they are not detected in the sample of the highest concentration (4 mg mL^{-1}). These large species are not further considered in the following analysis. The continuous sedimentation distribution ($c(s)$ versus s) was calculated using numerical solutions of the Lamm equation to fit the boundaries (*37*, *38*). In a first approach, the translational friction ratio (f/f_0) was treated as a fitting parameter and was determined through data analysis. Values of f/f_0 ranging from 1.7 to 2.1 were obtained for the different protein concentrations together with size distributions of the sedimentation coefficient centered on $s_{20,w}$ values ranging from 2.9 to 3.5 S. A spherical protein (f/f_0 = 1.25) of 65 kDa would have a $s_{20,w}$ value of 4.7 S, indicating that the P proteins are elongated. The $s_{20,w}$ value corresponding to the maximum of the size distribution varies little with protein concentration (data not shown), and thus, in a second approach, a value of f/f_0 for each protein was calculated by combining the most probable value of $s_{20,w}$, with the translational diffusion coefficient, $D_{20,w}$, measured by DLS or with the molecular mass, M_w, measured by MALLS (eqs 9a and 9b). This f/f_0 value was then used as a fixed parameter

Table 1: Molecular Mass of P Proteins Obtained by Different Methods[a]

	M_w (kDa)					
	from the sequence (for a dimer)	from MALLS	from AUC (*s*) and SEC (R_S)	from AUC (*s*) and DLS (*D*)	from SANS-Guinier	from SANS-*P*(*r*)
VSV P	61.952	61 ± 2	63 ± 5	61 ± 5	69 ± 4 (0.216 ± 0.008)	69 ± 5 (0.210 ± 0.017)
ST VSV P	62.018	63 ± 3	69 ± 5	67 ± 5	79 ± 5 (0.180 ± 0.012)	75 ± 5 (0.170 ± 0.012)
RV P	67.232	69 ± 2	71 ± 5	71 ± 5	81 ± 3 (0.255 ± 0.018)	78 ± 5 (0.253 ± 0.017)

[a] A value of the weight average molecular mass was obtained from MALLS data by averaging the molecular mass values calculated at each point of the chromatographic peak (Figure 1) using protein concentration measured by refractometry and the intensity of scattered light at 7 different angles (eq 4). A value was obtained from the sedimentation coefficient, *s*, measured by analytical ultracentrifugation (AUC) and either the Stokes radius, R_S, measured by SEC according to eq 8 or the diffusion coefficient measured by DLS according to eq 7. A value was obtained from the protein concentration, the scattering length density, and the intensity of neutron scattering at zero angle, $I(0)$ (SANS), either measured by extrapolating the Guinier plot to zero angle or from the analysis of the distance function distribution ($P(r)$), according to eq 13. Values in parentheses show $I(0)$ values in cm^{-1}.

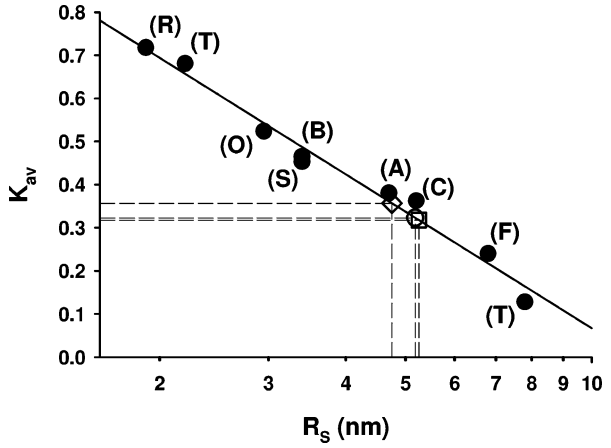

FIGURE 2: Stoke's radius (R_S) of VSV P, ST VSV P, and RV P proteins measured by size-exclusion chromatography. The figure shows the plot of K_{av} versus R_S. SEC was performed as described in Figure 1. Standard proteins (filled circles) used to calibrate the column were (T) thyroglobulin, (F) ferritine, (C) catalase, (A) aldolase, (S) serumalbumine, (O) ovalbumine, (T) α-chymotrypsinogen, and (R) RNAse A. Stokes radii are taken from Uversky (*35*). The line shows the linear fit ($K_{av} = 0.964 - 0.897 \log(R_S)$) with a correlation coefficient of 0.978. The open symbols show the measured K_{av} and calculated Stokes radii of VSV P (circle), ST VSV P (square), and RV P (diamond).

in the analysis of the data (Table 3). Figure 3 shows the plots of $c(s)$ versus *s* for the three P proteins obtained from this second analysis. For VSV P (Figure 3A) and ST VSV P (Figure 3B) the analysis yields a single symmetrical peak with *s* values of 2.8 ± 0.1 S ($s_{20,w} = 2.9$ S) and 3.0 ± 0.1 S ($s_{20,w} = 3.1$ S), respectively (Table 2), confirming the existence of monodisperse species. With RV P (Figure 3C), several species are observed. The major species that represents 65% of the molecules has an *s* value of 3.4 ± 0.1 S ($s_{20,w} = 3.5$ S). These experiments were performed in the absence of a reducing agent and several species with *s* values ranging from 4 to 12 S (35%) could correspond to the disulfide bridged forms observed by SEC. Combining *s* values measured by analytical centrifugation with values of M_w, *D*, or R_S determined by other methods yields self-consistent estimates of these different parameters (Tables 1 and 2). The values obtained with VSV P, ST VSV P, and the major form of RV P support the conclusion that P proteins form elongated dimers. The hydrodynamic parameters measured by the different methods are summarized in Table 2.

Overall Shape of P by Small-Angle Neutron Scattering. SANS experiments were used to characterize the molecular dimensions of the three P proteins. Guinier plots (Figure 4A) are linear for *Q* values ranging from 0.10 to 0.28 nm^{-1} ($0.5 < Q \cdot R_g < 1.5$) and yield model-independent values for the radii of gyration of 5.3 to 5.5 nm (Table 3). The scattered intensity extrapolated to zero angle, $I(0)$, provides an estimate of the molecular mass of the protein (Table 1) that is slightly higher than that measured by light scattering but remains in agreement with the molecular mass of dimers (Table 1). Similar R_g and M_w values are obtained from the size distribution function ($P(r)$) calculated for *Q* values ranging from 0.15 to 0.76 nm^{-1} (Figure 4C and Table 2). The discrepancy between molecular mass values measured by MALLS and SANS is larger for RV P than for VSV P and ST VSV P, possibly because of the presence of small amounts of larger species in the RV P samples. Cross-sectional Guinier plots (Figure 4B) are linear for *Q* value ranging from 0.22 to 0.75 nm^{-1} ($0.3 < Q \cdot R_c < 1.2$), an indication that the P proteins are elongated in one direction. The slope of these plots yielded the cross-sectional radii of gyration, R_c, of about 1.6−1.8 nm (Table 3). From R_g and R_c values, we calculated triaxial parameters for a cylinder (Table 3) (*41*). Values for the partial specific volumes calculated from the cylinder models and the molecular mass measured by MALLS are close to the values calculated from the amino acid composition of the proteins using Sedenterp.

Formation of Large Oligomers at 30 °C. Incubation of VSV P and ST VSV P at 30 °C induces the formation of larger oligomers that elute in the exclusion volume of our SEC column ($M_w > 700$ kDa) (Figure 5A). The conversion occurs in about 8 h, and no intermediate forms accumulate during the reaction. The kinetics of disappearance of dimeric P (Figure 5B) is identical to the kinetics of appearance of the large oligomeric species. Electron microscopy showed that both VSV P and ST VSV P form short oligomeric species after incubation at 30 °C for 1 h (Figure 6A) that grow into irregular filamentous structures after incubation for 3.5 h (Figure 6B). Both oligomers and filaments have an irregular diameter of about 6−8 nm, and it is not possible to visualize the organization of the P dimers in these filaments. Incubation of RV P at 30 °C also leads to the

Table 2: Hydrodynamic Properties of P Proteins Obtained by Different Methods[a]

			$D_{20,w}$ (10^{-7} cm s^{-2})			R_S (nm)		
	$s_{20,w}$ (S)	f/f_0	from DLS	from AUC (s) and MALLS (M_w)	from AUC (s) and SEC (R_S)	from SEC	from DLS	from AUC (s) and MALLS (M_w)
VSV P	2.9 ± 0.1	1.92	4.27 ± 0.08	4.27 ± 0.10	4.13 ± 0.10	5.2 ± 0.1	5.1 ± 0.1	5.0 ± 0.1
ST VSV P	3.1 ± 0.1	1.88	4.15 ± 0.08	4.41 ± 0.10	4.05 ± 0.10	5.3 ± 0.1	5.2 ± 0.1	4.9 ± 0.2
RV P	3.5 ± 0.1 (65%)	1.74	4.48 ± 0.10	4.60 ± 0.10	4.47 ± 0.10	4.8 ± 0.1	4.8 ± 0.1	4.7 ± 0.2

[a] The $s_{20,w}$ was obtained from the measured s value using eq 10a to correct for the viscosity and density of the buffer solution. The number within parentheses indicates the fraction of the major component of RV P. The f/f_0 is the frictional coefficient ratio used to fit the sedimentation velocity data. It corresponds to an average of the values calculated from a gross estimation of s and from M_w (MALLS) or D (DLS), according to eqs 9a and 9b, respectively. The diffusion coefficient, $D_{20,w}$, was measured by DLS and was calculated from the sedimentation coefficient, $s_{20,w}$, measured by analytical ultracentrifugation (AUC) and from either the molecular mass measured by MALLS or the Stokes radius measured by SEC, by combining eqs 7 and 8. The Stokes radius was measured by SEC, was calculated from the diffusion coefficient, $D_{20,w}$, according to eq 5, and was calculated by combining the sedimentation coefficient, $s_{20,w}$, measured by analytical ultracentrifugation (AUC) with the molecular mass measured by MALLS, according to eq 8.

Table 3: Molecular Dimensions of P Proteins Calculated from SANS Experiments[a]

	R_g (nm)					
	from SANS-Guinier	from SANS-$P(r)$	R_c (nm) from SANS-Guinier	D_{max} (nm)	L (nm)	r (nm)
VSV P	5.3 ± 0.1	5.4 ± 0.1	1.55 ± 0.02	17.0	17.6 ± 0.3	2.2 ± 0.1
ST VSV P	5.4 ± 0.1	5.5 ± 0.1	1.63 ± 0.02	17.5	17.8 ± 0.4	2.3 ± 0.1
RV P	5.5 ± 0.1	5.5 ± 0.1	1.76 ± 0.02	19.0	18.1 ± 0.3	2.5 ± 0.1

[a] The radius of gyration, R_g, was calculated from the initial slope of the Guinier plot ($\ln(I(Q))$ versus Q^2) or from the analysis of the distance distribution function ($P(r)$). The cross-sectional radius of gyration, R_c, was calculated from the slope of the plot of ($\ln(I(Q)\cdot Q)$ versus Q^2). D_{max} represents the optimal value obtained in the calculation of the distance distribution function that gave a R_g value in agreement with that from Guinier analysis. L and r represents the length and radius of model cylinder calculated from R_g and R_c values according to eqs 15 and 16.

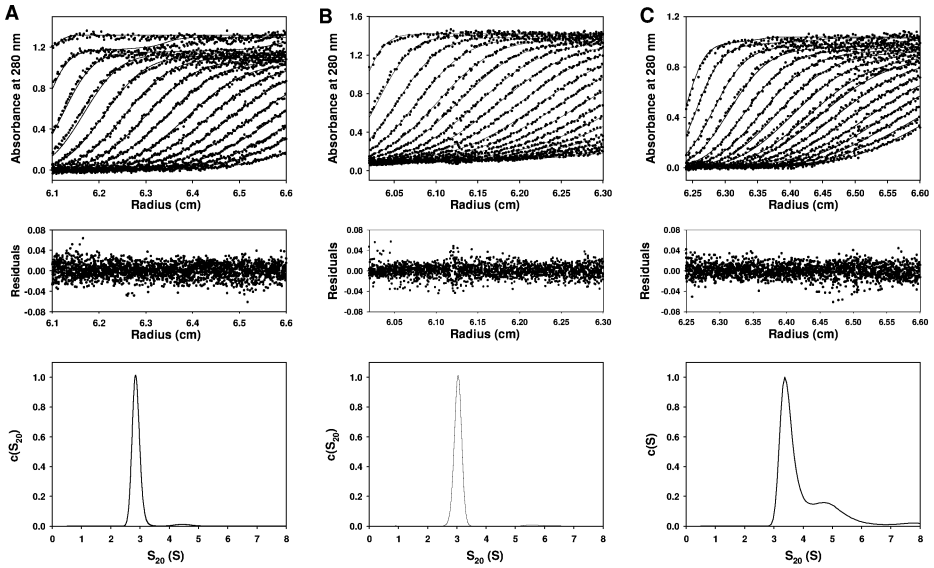

FIGURE 3: Sedimentation coefficient distribution calculated by modeling of sedimentation velocity concentration profiles. The figure shows the scans and fitting curves resulting from the analysis with Sedfit software (top panels), residuals of the fit (middle panels), and sedimentation coefficient distribution (bottom panels) for (A) VSV P, (B) ST VSV P, and (C) RV P. The sedimentation coefficients at the maximum of the distributions are 2.8 ± 0.1 S (VSV P WT), 3.0 ± 0.1 S (VSV P double mutant), and 3.7 ± 0.1 S (RV P WT). For all samples, the ultracentrifuge was run at 42 000 rpm and 20 °C. The buffer contained 20 mM Tris/HCl, 150 mM NaCl (pH 7.5). Cells were scanned at 280 nm.

formation of large filamentous oligomers but much more slowly, such that after incubation for 3.5 h only few were observed by electron microscopy.

DISCUSSION

Structural Properties of P Oligomers. Combining static light scattering detection with SEC, we clearly demonstrated that, in solution near neutral pH, the recombinant P proteins from VSV and RV form dimers. Since the VSV phosphoprotein was produced in bacteria and since its mass determined by mass spectrometry was that of the unphosphorylated protein, these observations suggest that phosphorylation is not necessary for dimerization. Static laser light scattering is a powerful tool for measuring absolute molecular mass of macromolecules and of multimolecular complexes (*36*, *37*). For particles smaller than the wavelength of the incident light, the intensity of scattered light extrapolated to zero angle is directly proportional to the molecular mass of the particle and to its concentration. Because it does not depend on calibration with globular proteins, this detection method is

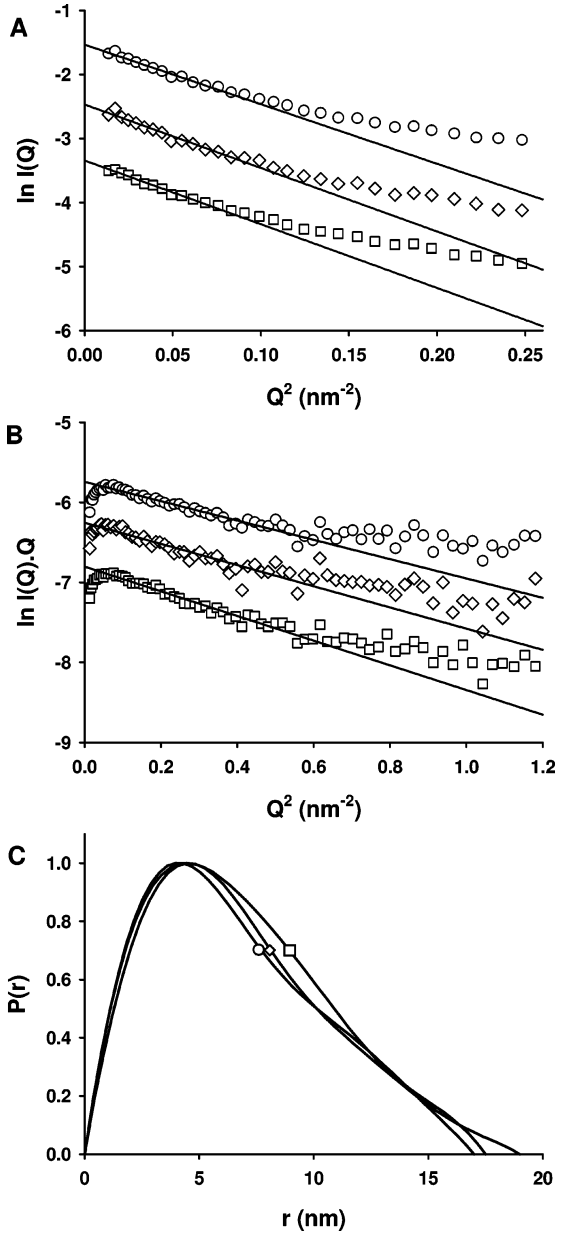

FIGURE 4: Small-angle neutron scattering analysis of phosphoproteins. (A) R_g Guinier plot (ln($I(Q)$) versus Q^2) for VSV P (circles), ST VSV P (diamonds), and RV P (squares). The fitted lines using $0.10 < Q < 0.28$ nm^{-1} yielded values for the radii of gyration of 5.3 ± 0.1 nm for VSV P, 5.4 ± 0.1 for ST VSV P, and 5.5 ± 0.1 for RV P. The fit corresponds to a range of $0.5 < Q \cdot R_g < 1.5$. The $I(0)$ value calculated from the intercept, together with protein concentrations, corresponds to molar mass of 69 000 ± 4000 for VSV P, 79 000 ± 5000 for ST VSV P, and 81 000 ± 3000 for RV P. For clarity, each plots is shifted along the ln($I(Q)$) axis. (B) Cross-sectional R_c Guinier plot (ln($I(Q) \cdot Q$) versus Q^2) for VSV P (circles), ST VSV P (diamonds), and RV P (squares). The fitted lines using $0.22 < Q < 0.75$ nm^{-1} yielded values for the cross-sectional radii of gyration of 1.55 ± 0.02 nm for VSV P, 1.63 ± 0.02, for ST VSV P, and 1.76 ± 0.01 for RV P. The fit thus corresponds to a range of $0.3 < Q \cdot R_c < 1.3$. For clarity, each plot is shifted along the ln($I(Q) \cdot Q$) axis. All samples were prepared in 20 mM Tris/HCl, 150 mM NaCl, pH 7.5, in 100% H_2O. Protein concentrations were close to 5 mg mL^{-1} . (C) Distance distribution function for VSV P (circle), ST VSV P (diamond), and RV P (square). The curve are calculated using the GNOM software, data for Q values ranging from 0.15 to 0.76 nm^{-1}, and D_{max} values reported in Table 3.

particularly suitable for determining the molecular mass of multimolecular complexes, or of elongated or partially

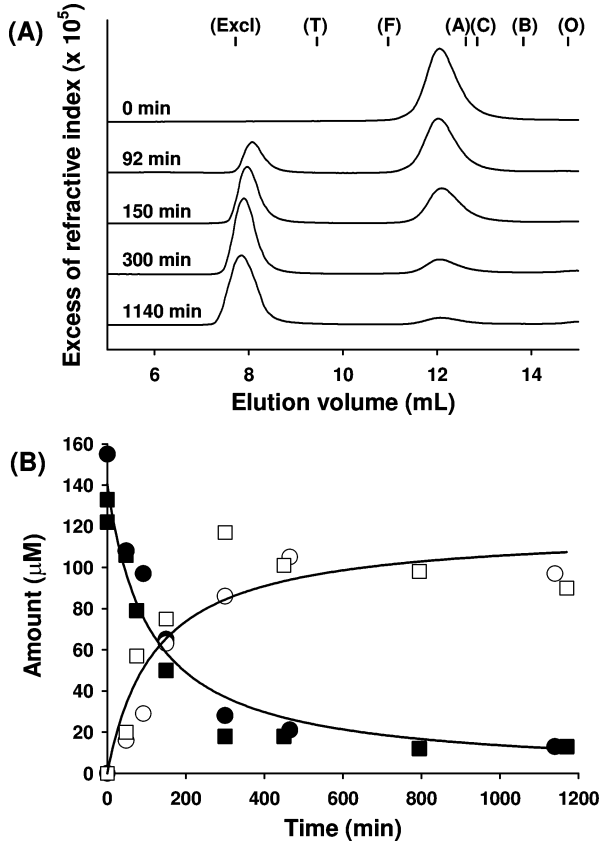

FIGURE 5: Kinetics of the oligomerization of VSV P at 30 °C. (A) Size exclusion chromatography profiles after different incubation times at 30 °C. VSV and ST VSV phosphoproteins at 2.6 mg/mL were incubated in 20 mM Tris/HCl, 150 mM NaCl at 30 °C pH 7.5. After different incubation times, 50 μL aliquots were injected on the column and monitored by refractometry. The elution volumes of standard globular proteins are shown at the top of the figure with labels as in Figure 2. (B) Kinetic curves. Peaks areas were converted to concentrations and plotted as a function of incubation time. Closed symbols are for dimers of VSV P (circles) and ST VSV P (squares), and open symbols are for oligomers eluting in the exclusion volume of the column (molar mass >1 × 10^6 g mol^{-1}). The data were fitted to a second-order equation (solid lines).

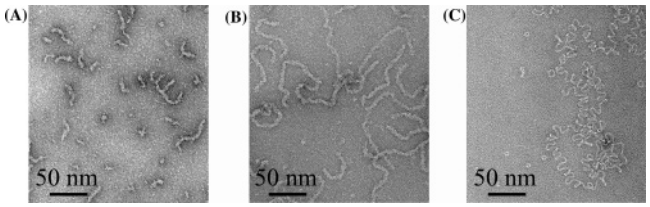

FIGURE 6: Electron microscopy of filamentous VSV P. Electron micrographs of negatively stained VSV P after 1 h (A) and 3.5 h (B) of incubation in 20 mM Tris/HCl, 150 mM NaCl, at pH 7.5 and 30 °C. Protein concentration during incubation at 30 °C was 2.6 mg mL^{-1}. (C) VSV ribonucleoprotein complex purified from infected cells and shown for comparison.

disordered proteins for which elution from size-exclusion chromatography columns is different from that of a globular protein. The combination with separation by SEC ensures that the measurement is not contaminated by the presence of small amounts of large aggregates. These results were confirmed by SANS experiments, in which the intensity extrapolated at zero angle is proportional to the molecular mass, which can thus be calculated on an absolute scale when the protein composition and concentration are known (*37*). Although SANS data were obtained without on-line separa-

tion by SEC, the molecular masses calculated from intensity at zero angle also show that P proteins form dimers (Table 1). We obtained similar results with ST VSV P (S60D/T62D variant) that was made to resemble a constitutively phosphorylated P protein, suggesting that phosphorylation does not induce oligomer formation or further oligomerization. The existence of dimers of P is in agreement with observations that two molecules of RV P bind per molecule of N in N°−P complexes (*43*), with the recent crystal structure of the central dimeric domain of VSV P protein (*23*), as well as with a previous study in which a combination of SEC and analytical centrifugation data indicated that RV P is larger than a monomer (*32*) and is consistent with a dimer (Y. Gaudin, personal communication). The Stokes radius of RV P (4.3 nm) measured in this previous study (*32*) is, however, significantly smaller than that measured here (4.8 nm). The results presented here contrast with previous work in which unphosphorylated VSV P was found to elute from a SEC column as a monomer (*19*, *24*, *25*), while phosphorylated forms of VSV P and ST VSV P were reported to form either dimers (*24*), trimers (*25*), or tetramers (*19*). Some of these experiments were carried out at lower protein concentrations (*24*, *25*), which could explain the observation of monomer, but the discrepancies and difficulties to obtain a clear-cut answer about the oligomeric state of *Rhabdoviridae* phosphoproteins arise from several peculiar properties of these proteins. First, P proteins exhibit an anomalous migration on SDS−PAGE, and thus, cross-linking experiments revealed by SDS−PAGE, although they demonstrate the existence of different forms of P, cannot be used to determine the accurate stoichiometry of the oligomers (*16*, *19*, *32*). Second, P protein oligomers are elongated and possibly partially disordered, rendering hydrodynamics measurements by SEC and analytical centrifugation difficult to interpret in the absence of an absolute measurement of the molecular mass. Third, VSV P and ST VSV P convert rapidly into soluble large oligomeric species upon incubation at 30 °C. For example, in the His-tag dilution assays used to demonstrate the oligomerization induced by phosphorylation (*16*, *19*) the protein was incubated at 32 °C for 30 min. All experiments that involved a long incubation time above 25 °C should thus be taken with caution. Similar difficulties were encountered for determining the stoichiometry of P oligomers from Sendai and mumps viruses (*Paramyxoviridae*). Sendai virus P protein has been reported to form trimers (*11*), until it was demonstrated that it forms tetramers (*44*, *45*). With Chandipura virus (CHPV), phosphorylation of a single residue stabilizes the dimers (*16*), but it has been found recently that different oligomeric forms of unphosphorylated P also coexist in a concentration-dependent equilibrium (*28*).

The P proteins from VSV and RV exhibit an elongated rodlike shape as suggested by the large Stokes radii measured by SEC and as confirmed by the large frictional ratio obtained from the sedimentation velocity experiments and by the shape of the cross-sectional Guinier plots. The results obtained by sedimentation velocity, dynamic light scattering, and size-exclusion chromatography agree with dimers exhibiting a hydrodynamic radius of 4.8−5.3 nm and a frictional ratio of 1.7−1.9. SANS experiments yielded a radius of gyration of about 5.3−5.5 nm and a cross-sectional radius of gyration of about 1.6−1.8 nm for the three phosphoproteins, which indicated elongated molecules with one axis 8−7 times longer than the other two. Assuming a cylindrical shape, triaxial parameters, the radius, r, and the length, L, can be calculated from the values of R_g and R_c (Table 3). The theoretical frictional ratio (f/f_0) calculated for a cylinder of such dimensions ranges from 1.3 to 1.9 (*46*). The partial specific volume of the proteins calculated for such hypothetical cylinders indicates that, for VSV P, the protein occupied 96% of the volume. For RV P, the triaxial parameters, as the molecular mass (see above), were possibly overestimated because of the presence of larger species in the sample. The experimental factor $\delta = R_g/R_S$ is a sensitive indicator of the compactness of the molecule. The values found here range from 1.0 to 1.2. Its value is 0.775 for a compact sphere, 0.8 for a globular protein (*47*), about 0.9 for a molten globule (*48*), and 1.5 for a Gaussian coil (*49*). The theoretical R_g/R_S ratio calculated for a cylindrical shape of dimensions similar to those of P proteins ranges from 0.70 to 1.20 (*50*). Recent studies have concluded that P proteins from *Paramyxoviridae* viruses are intrinsically disordered proteins (IDPs) (*51*, *52*) with structured domains separated by long disordered regions (*53*, *54*). RV and VSV P are sensitive to proteolytic digestion, and analysis of the amino acid sequence suggested that P proteins from *Rhabdoviridae* viruses also belong to this class of proteins (*51*). Therefore, both an elongated shape and the flexibility inherent to the presence of long disordered regions can explain a R_g/R_S ratio close to unity. Also, it is noteworthy that a truncated form of Sendai virus P, which contains the central tetramerization domain and the C-terminal N-RNA binding domain (PCT), exhibits similar shape and molecular dimensions (*45*, *55*). The structure of the dimerization domain of VSV, however, reveals that interactions between P molecules in these dimers do not occur through the formation of a long coiled-coil, but rather through central contacts between an α-helix from each monomer and the formation of two intermolecular β-sheets on the sides (*23*). For RV P, secondary structure prediction algorithms also predict α-helices in the central region rather than a coiled-coil, suggesting a structural organization for this domain similar to that of VSV (data not shown).

Implications for Viral RNA Synthesis. With both VSV and CHPV, phosphorylation of residues in the N-terminal domain of P proteins or replacements of these residues by acidic residues have been correlated with transcription activity (*16*, *19*). Recent data obtained with VSV suggest that two distinct multimolecular complexes carry out RNA transcription and replication (*26*, *27*) and initiate RNA synthesis at different sites on the genome (*56*). Multiple results suggest that phosphorylation of P protein from VSV and from CHPV regulates the switch between transcription and replication and that the molecular origin of this change in activity resides in a change in conformation (*29*, *57*) and self-assembly of the P protein (*16*, *19*). Phosphorylation of different residues in the N- and C-terminal domains of VSV P are essential for viral growth (*58*). Phosphorylation in the C-terminal domain might control replication (*59*), whereas phosphorylation in the N-terminal domain is necessary for transcription activation (*18*, *20*, *60*) but not for replication (*60*). Replacements of phosphorylation sites in the N-terminal domain by alanine can severely impair transcription activity (*21*, *60*), whereas replacements by glutamate or aspartate residues yield proteins that are constitutively active in transcription

(*15*, *19*, *60*). In particular, it has been reported that the double mutant S60D/T62D of VSV P (ST VSV P) mimics phosphorylation by constitutively producing oligomeric species (*19*). Phosphorylation of one residue in CHPV N-terminal domain has also been shown to control transcription (*30*). Here, however, we show that unphosphorylated P proteins from VSV and RV as well as the mutant of VSV (S60D/T62D) that is constitutively active in transcription (*19*, *60*) form dimers. Although phosphorylation seems to be required for transcription activation, our results suggest that phosphorylation and transcriptional activation do not need oligomeric structures larger than a dimer, and that self-association of phosphorylated P is not involved in controlling the transcription/replication switch. Alternatively, it is possible that the addition of negative charges in a highly acidic region of P proteins through phosphorylation or mutation might affect the conformation of P (*29*), its dynamics, or its affinity for another component of the transcription or replication complexes (*15*). Interactions of P proteins with the leader RNA could also play an important role in the regulation of the replication and transcription activities (*28*), and phosphorylation of P could also affect these interactions.

Finally, we showed that both VSV P and ST VSV P form filamentous oligomers of larger size (>700 kDa) when incubated at 30 °C. The conversion is cooperative, and no intermediate of small size accumulates during the process. Mutations of the phosphorylation sites have no effect on the kinetics of the oligomerization. In the previous studies (*19*), phosphorylation has been performed by incubation of P in the presence of casein kinase II for 45 min or more at 32 °C, and thus, it is possible that the appearance of the higher molecular weight forms was attributed wrongly to the formation of tetramers. These filamentous species form under physiological temperatures, and it is now of major interest to understand whether or not they play a relevant role in the replication of the virus and interact with the viral ribonucleoprotein complex (Figure 6C). Additional binding of Sendai virus P protein to N:RNA template is required for stimulating the activity of the RNA polymerase complex (*61*), and it will thus be important to verify if such filamentous forms of P are involved in the replication processes under physiological conditions.

ACKNOWLEDGMENT

We thank Danielle Blondel (Unite Mixte de Virologie Moleculaire et Structurale, Gif sur Yvette) for the plasmid encoding the VSV P protein and the sample of VSV RNP; Bertrand Lefèbvre, Denis Daveloos, and Bernard Brasmes (CRSSA, Grenoble) for mass spectrometry measurements; and Christine Ebel (IBS, Grenoble) for the use of the analytical centrifuge and discussion of the results.

REFERENCES

1. Fields, B. N., Knipe, D. M., Howley, P. M., Chanock, R. M., Melnik, T. P., Roizman, B., and Straus, S. E. (1996) *Fields' virology*, 3rd ed., Lippincott-Raven Publishers, New York.
2. Albertini, A. A., Wernimont, A. K., Muziol, T., Ravelli, R. B., Clapier, C. R., Schoehn, G., Weissenhorn, W., and Ruigrok, R. W. (2006) Crystal structure of the rabies virus nucleoprotein-RNA complex, *Science 313*, 360−363.
3. Green, T. J., Zhang, X., Wertz, G. W., and Luo, M. (2006) Structure of the vesicular stomatitis virus nucleoprotein-RNA complex, *Science 313*, 357−360.
4. Arnheiter, H., Davis, N. L., Wertz, G., Schubert, M., and Lazzarini, R. A. (1985) Role of the nucleocapsid protein in regulating vesicular stomatitis virus RNA synthesis, *Cell 41*, 259−267.
5. Emerson, S. U., and Yu, Y. (1975) Both NS and L proteins are required for in vitro RNA synthesis by vesicular stomatitis virus, *J. Virol. 15*, 1348−1356.
6. Pattnaik, A. K., and Wertz, G. W. (1990) Replication and amplification of defective interfering particle RNAs of vesicular stomatitis virus in cells expressing viral proteins from vectors containing cloned cDNAs, *J. Virol. 64*, 2948−2957.
7. Gupta, A. K., and Banerjee, A. K. (1997) Expression and purification of vesicular stomatitis virus N-P complex from Escherichia coli: role in genome RNA transcription and replication in vitro, *J. Virol. 71*, 4264−4271.
8. Masters, P. S., and Banerjee, A. K. (1988) Complex formation with vesicular stomatitis virus phosphoprotein NS prevents binding of nucleocapsid protein N to nonspecific RNA, *J. Virol. 62*, 2658−2664.
9. Banerjee, A. K. (1987) Transcription and replication of rhabdoviruses, *Microbiol. Rev. 51*, 66−87.
10. Emerson, S. U., and Wagner, R. R. (1973) L protein requirement for in vitro RNA synthesis by vesicular stomatitis virus, *J. Virol. 12*, 1325−1335.
11. Curran, J., Boeck, R., Lin-Marq, N., Lupas, A., and Kolakofsky, D. (1995) Paramyxovirus phosphoproteins form homotrimers as determined by an epitope dilution assay, via predicted coiled coils, *Virology 214*, 139−149.
12. Kolakofsky, D., Le Mercier, P., Iseni, F., and Garcin, D. (2004) Viral DNA polymerase scanning and the gymnastics of Sendai virus RNA synthesis, *Virology 318*, 463−473.
13. Barik, S., Mc, Lean, T., and Dupuy, L. C. (1995) Phosphorylation of Ser^{232} directly regulates the transcriptional activity of the P protein of human respiratory syncytial virus: phosphorylation of Ser^{237} may play an accessorry role, *Virology 213*, 405−412.
14. Asenjo, A., and Villanueva, N. (2000) Regulated but not constitutive human respiratory syncytial virus (HRSV) P protein phosphorylation is essential for oligomerization, *FEBS Lett. 467*, 279−284.
15. Gao, Y., and Lenard, J. (1995) Cooperative binding of multimeric phosphoprotein (P) of vesicular stomatitis virus to polymerase (L) and template: pathways of assembly, *J. Virol. 69*, 7718−7723.
16. Raha, T., Samal, E., Majumdar, A., Basak, S., Chattopadhyay, D., and Chattopadhyay, D. J. (2000) N-terminal region of P protein of Chandipura virus is responsible for phosphorylation-mediated homodimerization, *Protein Eng. 13*, 437−444.
17. Chen, M., Ogino, T., and Banerjee, A. K. (2006) Mapping and functional role of the self-association domain of vesicular stomatitis virus phoshoprotein, *J. Virol. 80*, 9511−9518.
18. Barik, S., and Banerjee, A. K. (1992) Phosphorylation by cellular casein kinase II is essential for transcriptional activity of vesicular stomatitis virus phosphoprotein P, *Proc. Natl. Acad. Sci. U.S.A. 89*, 6570−6574.
19. Gao, Y., and Lenard, J. (1995) Multimerization and transcriptional activation of the phosphoprotein (P) of vesicular stomatitis virus by casein kinase-II, *EMBO J. 14*, 1240−1247.
20. Barik, S., and Banerjee, A. K. (1992) Sequential phosphorylation of the phosphoprotein of vesicular stomatitis virus by cellular and viral protein kinases is essential for transcription activation, *J. Virol. 66*, 1109−1118.
21. Spadafora, D., Canter, D. M., Jackson, R. L., and Perrault, J. (1996) Constitutive phosphorylation of the vesicular stomatitis virus P protein modulates polymerase complex formation but is not essential for transcription or replication, *J. Virol. 70*, 4538−4548.
22. Peluso, R. W., and Moyer, S. A. (1988) Viral proteins required for the in vitro replication of vesicular stomatitis virus defective interfering particle genome RNA, *Virology 162*, 369−376.
23. Ding, H., Green, T. J., Lu, S., and Luo, M. (2006) Crystal structure of the oligomerization domain of the phosphoprotein of vesicular stomatitis virus, *J. Virol. 80*, 2808−2814.
24. Das, T., Gupta, A. K., Sims, P. W., Gelfand, C. A., Jentoft, J. E., and Banerjee, A. K. (1995) Role of cellular casein kinase II in the function of the phosphoprotein (P) subunit of RNA polymerase of vesicular stomatitis virus, *J. Biol. Chem. 270*, 24100−24107.
25. Gao, Y., Greenfield, N. J., Cleverley, D. Z., and Lenard, J. (1996) The transcriptional form of the phosphoprotein of vesicular stomatitis virus is a trimer: structure and stability, *Biochemistry 35*, 14569−14573.

26. Qanungo, K. R., Shaji, D., Mathur, M., and Banerjee, A. K. (2004) Two RNA polymerase complexes from vesicular stomatitis virus-infected cells that carry out transcription and replication of genome RNA, *Proc. Natl. Acad. Sci. U.S.A. 101*, 5952−5957.
27. Gupta, A. K., Shaji, D., and Banerjee, A. K. (2003) Identification of a novel tripartite complex involved in replication of vesicular stomatitis virus genome RNA, *J. Virol. 77*, 732−738.
28. Basak, S., Polley, S., Basu, M., Chattopadhyay, D., and Roy, S. (2004) Monomer and dimer of Chandipura virus unphosphorylated P-protein binds leader RNA differently: implications for viral RNA synthesis, *J. Mol. Biol. 339*, 1089−1101.
29. Raha, T., Chattopadhyay, D., Chattopadhyay, D., and Roy, S. (1999) A phosphorylation-induced major structural change in the N-terminal domain of the P protein of Chandipura virus, *Biochemistry 38*, 2110−2116.
30. Chattopadhyay, D., Raha, T., and Chattopadhyay, D. (1997) Single serine phosphorylation within the acidic domain of Chandipura virus P protein regulates the transcription in vitro, *Virology 239*, 11−19.
31. Chattopadhyay, D., and Chattopadhyay, D. (1994) *Cell. Mol. Biol. Res. 40*, 693−698.
32. Gigant, B., Iseni, F., Gaudin, Y., Knossow, M., and Blondel, D. (2000) Neither phosphorylation nor the amino-terminal part of rabies virus phosphoprotein is required for its oligomerization, *J. Gen. Virol. 81*, 1757−1761.
33. Mavrakis, M., McCarthy, A. A., Roche, S., Blondel, D., and Ruigrok, R. W. (2004) Structure and function of the C-terminal domain of the polymerase cofactor of rabies virus, *J. Mol. Biol. 343*, 819−831.
34. Prehaud, C., Nel, K., and Bishop, D. H. (1992) Baculovirus-expressed rabies virus M1 protein is not phosphorylated: it forms multiple complexes with expressed rabies N protein, *Virology 189*, 766−770.
35. Uversky, V. N. (1993) Use of fast protein size-exclusion liquid chromatography to study the unfolding of proteins which denature through the molten globule, *Biochemistry 32*, 13288−13298.
36. Wyatt, P. J. (1998) Submicrometer Particle Sizing by Multiangle Light Scattering following Fractionation, *J. Colloid Interface Sci. 197*, 9−20.
37. Serdyuk, I. N., Zaccai, N. R., and Zaccai, J. (2007) *Methods in Molecular Biophysics: Structure, Dynamics, Function*, Cambridge University Press, Cambridge.
38. Schuck, P. (2000) Size-distribution analysis of macromolecules by sedimentation velocity ultracentrifugation and lamm equation modeling, *Biophys. J. 78*, 1606−1619.
39. Svedberg, T. H., and Pedersen, K. O. (1940) *The Ultracentrifuge*, Oxford University Press, Oxford.
40. Jacrot, B., and Zaccai, G. (1981) Determination of molecular weight by neutron scattering, *Biopolymers 20*, 2413−2426.
41. Glatter, O., and Kratky, O. (1982) *Small Angle X-ray Scattering*, Academic Press, London, U.K.
42. Semenyuk, A. V., and Svergun, D. (1991) GNOM - a program package for small-angle scattering data processing, *J. Appl. Crystallogr. 24*, 537−540.
43. Mavrakis, M., Iseni, F., Mazza, C., Schoehn, G., Ebel, C., Gentzel, M., Franz, T., and Ruigrok, R. W. (2003) Isolation and characterisation of the rabies virus N degrees-P complex produced in insect cells, *Virology 305*, 406−414.
44. Tarbouriech, N., Curran, J., Ruigrok, R. W., and Burmeister, W. P. (2000) Tetrameric coiled coil domain of Sendai virus phosphoprotein, *Nat. Struct. Biol. 7*, 777−781.
45. Tarbouriech, N., Curran, J., Ebel, C., Ruigrok, R. W., and Burmeister, W. P. (2000) On the domain structure and the polymerization state of the sendai virus P protein, *Virology 266*, 99−109.
46. Bloomfield, V., Dalton, W. O., and Van Holde, K. E. (1967) Frictional coefficients of multisubunit structures. I. Theory, *Biopolymers 5*, 135−148.
47. Damaschun, G., Damaschun, H., Gast, K., Misselwitz, R., Zirwer, D., Guhrs, K. H., Hartmann, M., Schlott, B., Triebel, H., and Behnke, D. (1993) Physical and conformational properties of staphylokinase in solution, *Biochim. Biophys. Acta 1161*, 244−248.
48. Gast, K., Damaschun, H., Misselwitz, R., Muller-Frohne, M., Zirwer, D., and Damaschun, G. (1994) Compactness of protein molten globules: temperature-induced structural changes of the apomyoglobin folding intermediate, *Eur. Biophys. J. 23*, 297−305.
49. Tanford, C. (1961) *Physical chemistry of macromolecules*, New York.
50. Santos, N. C., and Castanho, M. A. R. B. (1996) Teaching light scattering spectroscopy: The dimension and shape of tabacco mosaic virus, *Biophys. J. 71*, 1641−1650.
51. Karlin, D., Ferron, F., Canard, B., and Longhi, S. (2003) Structural disorder and modular organization in Paramyxovirinae N and P, *J. Gen. Virol. 84*, 3239−3252.
52. Bourhis, J. M., Canard, B., and Longhi, S. (2006) Structural disorder within the replicative complex of measles virus: functional implications, *Virology 344*, 94−110.
53. Radivojac, P., Obradovic, Z., Smith, D. K., Zhu, G., Vucetic, S., Brown, C. J., Lawson, J. D., and Dunker, A. K. (2004) Protein flexibility and intrinsic disorder, *Protein Sci. 13*, 71−80.
54. Dyson, H. J., and Wright, P. E. (2005) Intrinsically unstructured proteins and their functions, *Nat. Rev. Mol. Cell Biol. 6*, 197−208.
55. Blanchard, L., Tarbouriech, N., Blackledge, M., Timmins, P., Burmeister, W. P., Ruigrok, R. W., and Marion, D. (2004) Structure and dynamics of the nucleocapsid-binding domain of the Sendai virus phosphoprotein in solution, *Virology 319*, 201−211.
56. Whelan, S. P., and Wertz, G. W. (2002) Transcription and replication initiate at separate sites on the vesicular stomatitis virus genome, *Proc. Natl. Acad. Sci. U.S.A. 99*, 9178−9183.
57. Gupta, A. K., Blondel, D., Choudhary, S., and Banerjee, A. K. (2000) The phosphoprotein of rabies virus is phosphorylated by a unique cellular protein kinase and specific isomers of protein kinase C, *J. Virol. 74*, 91−98.
58. Das, S. C., and Pattnaik, A. K. (2004) Phosphorylation of vesicular stomatitis virus phosphoprotein P is indispensable for virus growth, *J. Virol. 78*, 6420−6430.
59. Hwang, L. N., Englund, N., Das, T., Banerjee, A. K., and Pattnaik, A. K. (1999) Optimal replication activity of vesicular stomatitis virus RNA polymerase requires phosphorylation of a residue(s) at carboxy-terminal domain II of its accessory subunit, phosphoprotein P, *J. Virol. 73*, 5613−5620.
60. Pattnaik, A. K., Hwang, L., Li, T., Englund, N., Mathur, M., Das, T., and Banerjee, A. K. (1997) Phosphorylation within the amino-terminal acidic domain I of the phosphoprotein of vesicular stomatitis virus is required for transcription but not for replication, *J. Virol. 71*, 8167−8175.
61. Curran, J. (1996) Reexamination of the Sendai virus P protein domains required for RNA synthesis: a possible supplemental role for the P protein, *Virology 221*, 130−140.

BI7007799